# A Multiband Microwave Photonic Filter Based on a Strongly Coupled Microring Resonator With Adjustable Bandwidth

Yuan Chen, ZhiQiang Fan, *Member, IEEE*, Yue Lin, Di Jiang, Xiang Li, and Qi Qiu

***Abstract*—A bandwidth-tunable multiband microwave photonic filter (MPF) using a strongly coupled microring resonator (MRR) with optical phase modulation is demonstrated theoretically and experimentally. Two notches of the MRR adjacent to the optical carrier break the intrinsic balance of the phase-modulated signal and then two sub-MPFs are formed thanks to the conversion from phase modulation to intensity modulation (PM-IM). The frequency responses of the two sub-MPFs are superimposed to form a passband with a fixed center frequency. Due to the periodicity of the MRR transmission spectrum, multiple passbands separated by a certain spacing appear in the frequency domain and combine to form a multiband MPF, whose bandwidth can be adjusted by tuning the wavelength of the carrier. The tunable bandwidth and shape factors ranging from 0.73 GHz to 2.73 GHz and 5.06 to 1.38 are experimentally performed. The number of passbands can be reconfigured. The proposed multiband MPF has the potential to be employed in modern multi-standard wireless communication systems.**

***Index Terms*—Microwave photonic filter, multiband filter, comb filter, microring resonator, phase modulation to intensity modulation conversion (PM-IM).**

## I. Introduction

With the rapid development and increasingly widespread application of wireless communication technology, communication standards have emerged to adapt to different scenarios or applications, gradually integrating many communication function modules into one communication terminal [1], [2]. In most cases, one type of communication protocol is not limited to only one frequency band (e.g., WLAN (2.4/5 GHz) and 5G (3.3–3.6/4.8–5 GHz for China)) [3]. In designing future mobile communication systems, the requirements of multi-standard and multi-service systems need to be met, and more compact size is preferred. Under such circumstances, multifunctional and multiband devices are ideal choices, where microwave filters are key components for frequency selection. Nowadays, spectrum needs are growing, but spectrum resources are limited, and the electromagnetic environment has become increasingly complex. Against this backdrop, research on wideband, high frequency, anti-interference, and integrability multiband filters help meet the urgent needs of various wireless communication systems, including satellite communication, transceivers, radio frequency identification (RFID), etc. [4], [5], [6], [7]. In addition, comb-like multiband filters are also applied in spectrum processing, signal generation, and removal of periodic noise and harmonic interference [8], [9], [10], [11].

Microwave photonic filters (MPFs) are promising candidates for RF signal processing due to their advantages, covering wide operation bandwidth, excellent tunability, reconfigurability/programmability, and electromagnetic interference immunity. Most MPFs reported are single-band ones, because such design is simpler and easier to realize tuning and reconfiguration features than multiband filters [12], [13], [14]. In recent years, reports on multiband MPFs have been more based on optical spectral slicing, optical frequency combs, and phase modulation to intensity modulation (PM-IM) [15], [16], [17]. However, several kilometers of fiber are required as dispersion media or delay lines in these schemes and some systems even require multiple laser sources or optical filters, which enlarges the size and complexity of the systems. Microring resonators (MRRs), as an integrated optical component, are extensively employed in many fields thanks to their small size, high Q value, and mass production. Its loopback structure, enables it to support multiple resonances, and the spacing between them, called free spectral range (FSR, $FSR = \lambda^2/(L \cdot n_g)$), is dependent on the loop length [18]. However, relevant studies based on its periodic resonances characteristics to form a multiband MPF are rare.

This paper theoretically and experimentally demonstrates a bandwidth tunable multiband MPF. Due to the PM-IM conversion and the periodic nature of the MRR spectrum, the optical carrier is paired with notches on both sides of it to form sub-MPFs. Multiple passbands separated by one FSR are constituted by the overlapping RF response of them. The bandwidth can be tuned by changing the wavelength of the optical carrier to vary the center frequencies of the sub-MPFs. Unlike conventional multiband MPF and MRR-based MPF schemes, it is the first time to form passbands and change the bandwidth of a multiband filter in this way. The multiband MPF consists of a tunable laser source (TLS), a phase modulator (PM), an

Manuscript received 11 January 2023; accepted 15 January 2023. Date of publication 18 January 2023; date of current version 30 January 2023. This work was supported by the National Natural Science Foundation of China under Grant 61971110. *(Corresponding author: Qi Qiu.)*

The authors are with the School of Optoelectronic Science and Engineering, University of Electronic Science and Technology of China, Chengdu 610054, China (e-mail: cy136798606@163.com; zqfan@uestc.edu.cn; linyue0204@163.com; jiangdi0313@gmail.com; lixiang3661@163.com; qqiu@uestc.edu.cn).

Digital Object Identifier 10.1109/JPHOT.2023.3237843

MRR, and a photodetector (PD). The application of a single laser source benefits greatly from skirting optical power mismatches between lasers and reducing the number of devices such as optical couplers and wavelength division multiplexers (WDMs). The introduction of a single MRR contributes to the integration and the thermal crosstalk problem common in multiple-MRRs MPF is eliminated. Because bias control is not required, phase modulation can eliminate the bias drift problem. The system stands out with a simple, compact and reliable structure, and lower optical power budgets. Experimental evaluation showed that the bandwidth tuning range of the proposed multiband MPF is 0.73-2.73 GHz. During the tuning, the shape factor of the passband was improved from 5.06 to 1.38. Experiments also showed that compared with the traditional microwave multiband filter, the proposed multiband MPF exhibited the following advantages: high operating frequency, wide tuning ranges of bandwidth and shape factor, good response consistency of each passband, flat-top filtering, and the ability to reconfigure the number of passbands [19], [20], [21].

## II. Principle

Fig. 1(a) illustrates the schematic diagram of the proposed MRR-based multiple passbands MPF. The optical carrier from the TLS with an angular frequency of $\omega_0$ is sent to the PM, where it is phase modulated by an RF signal with an $\omega_e$ angular frequency. Only $\pm 1$ sideband requires consideration under small signal modulation, and the optical field after PM is expressed as:

$$E_{PM} = E_0 J_0(\beta)\cdot e^{j(\omega_0 t)} + E_0 J_1(\beta)\cdot\left[e^{j(\omega_0+\omega_e)t} - e^{j(\omega_0-\omega_e)t}\right] \tag{1}$$

where $E_0$ stands for the amplitude of the input light, $J_n$(n = 01) the nth-order Bessel function of the first kind. $\beta = \pi V_{RF}/V_\pi$ is the phase modulation index, where $V_{RF}$ and $V_\pi$ serve as the magnitude of the RF signal and the half-wave voltage of the PM, respectively. Equation (1) confirms the generation of the upper and lower sidebands with equal amplitude but 180° phase shift. Therefore, the direct application of the PD to detect the phase-modulated signal, generates only a direct current (DC).

In order to break this anti-phase symmetry, an MRR is employed to tailor the optical phase-modulated signal. The optical frequency response of MRR can change the amplitude and phase of optical carrier and the two sidebands, as shown in Fig. 1(a) point A. The transfer function of MRR at the through port, which is derived from the transfer matrix method, is expressed as follows [22]:

$$\begin{cases} T(\theta) = \left|\frac{t-\alpha e^{i\theta}}{1-\alpha t e^{i\theta}}\right| \\ \Phi(\theta) = \pi + \theta + \tan^{-1}\left(\frac{t\sin\theta}{\alpha - t\cos\theta}\right) + \tan^{-1}\left(\frac{\alpha t\sin\theta}{1-\alpha t\cos\theta}\right) \end{cases} \tag{2}$$

where $T(\theta)$ and $\Phi(\theta)$ refer to the amplitude and phase response of the MRR at the loop phase shift $\theta$, which is expressed as $\theta = 2\pi n_{eff} L\omega_0/c$. Among them, $n_{eff}$ and $L$ denote the effective index and perimeter of MRR, respectively, $t$ and $\alpha$ the transmission coefficient in the coupling region and the round-trip transmittance (lossless: $t^2+k^2 = 1$, $\alpha = 1$), while c the angular frequency and the speed of light in vacuum, respectively. The phase-modulated signal transmitted through the MRR can be further described as

$$\begin{aligned} E_{PM-MRR} = E_0 \Big\{ & T(\omega_0)J_0(\beta)e^{i[\omega_0 t+\Phi(\omega_0)]} \\ & + T(\omega_0+\omega_e)J_1(\beta)e^{i[(\omega_0+\omega_e)t+\Phi(\omega_0+\omega_e)]} \\ & - T(\omega_0-\omega_e)J_1(\beta)e^{i[(\omega_0-\omega_e)t+\Phi(\omega_0-\omega_e)]} \Big\} \end{aligned} \tag{3}$$

After considering the amplitude and phase response of the MRR, the optical signal is fed to a high-speed PD and the photocurrent is sent to a vector network analyzer (VNA) for analysis. The RF response of the sub MPFs formed by different notches of strongly coupled MRR is superimposed to form multiple wide passbands through PM-IM conversion. The passband bandwidth depends on the relative position of the optical carrier and the two notches, which is the spacing between the center frequencies of the two sub-MPFs, as shown in Fig. 1(a) point B. The results

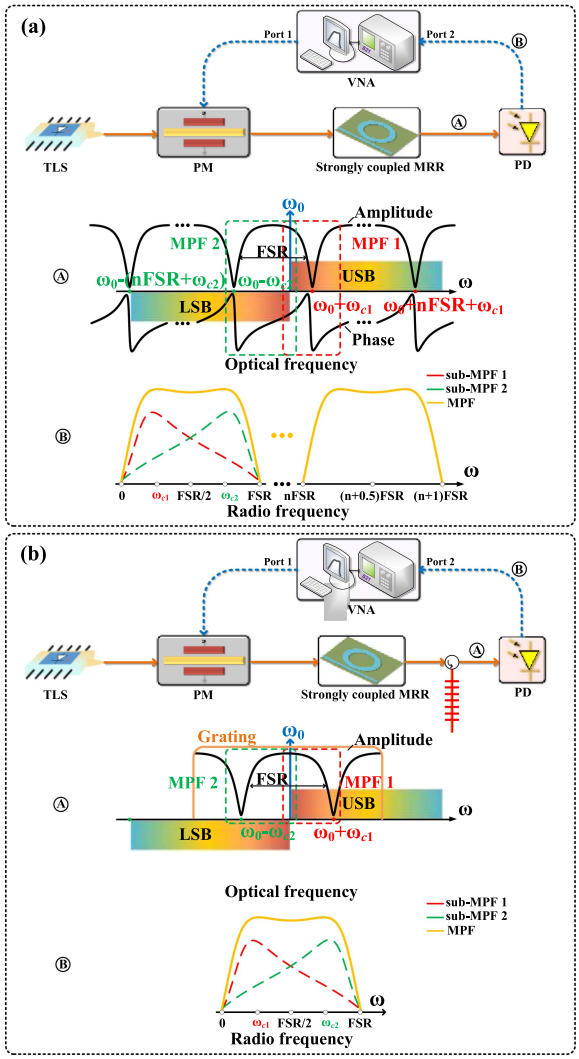


Fig. 1. Schematic diagram of the proposed MRR-based MPF without grating (a) and with grating (b).

can be presented as

$$i_{RF} = 2\eta T(\omega_0)|E_0|^2 J_0(\beta)J_1(\beta)\cdot \{T(\omega_0+\omega_e)\cos[\omega_e t+\Phi(\omega_0+\omega_e)-\Phi(\omega_0)] -T(\omega_0-\omega_e)\cos[\omega_e t+\Phi(\omega_0)-\Phi(\omega_0-\omega_e)]\} \quad (4)$$

where $\eta$ represents the responsibility of the PD. As seen from (4) and points A and B in Fig. 1(a), the output of the PD is affected by both the amplitude and the phase response of the MRR.

The coupling coefficient k serves as a critical parameter of the MRR, which directly affects the transmission spectrum of MRR. In general, a larger coupling coefficient leads to wider notch bandwidth of MRR. However, the FSR of the MRR is immune to the coupling coefficient, indicating the direct proportion between the coupling and the ratio of the notch bandwidth to the FSR [23]. When the coupling coefficient k of the MRR is large enough, the bandwidth of the notch is only slightly smaller than FSR and the phase start to change gently at 0.5 FSR below the resonance frequency, as shown in the inset of Fig. 2(b) (The optical frequency at a notch is assumed to be $\omega_{0n}$). That means the amplitude and phase response induced by MRR cannot be ignored even if the optical carrier and the two sidebands are far away from resonances. The above-mentioned factors break the symmetry of the sidebands outside the resonance, so that the frequency response of the sub-MPFs are no longer directly mapped from the transmission of the MRR through the PM-IM conversion, which leads to the change in their bandwidth and shape, and the contribution to the formation of the proposed MPF wide passbands. Owing to the periodic arrangement of MRR notches at the interval of the FSR, the S21 response of the MRR-based MPF is periodic with the FSR, and the analysis of the S21 response of MPF in one FSR helps to elaborate the working principle of the multiband MPF. Fig. 2(a) and 2(b) demonstrate the simulation results of the proposed MPF. When the $\omega_e$ ranges from 0 to an FSR, the bandpass envelopes of two sub-MPFs are superimposed to form a wideband bandpass MPF with a center frequency of 0.5 FSR. The bandwidth of the MPF is influenced by the relative position of the optical carrier and the two adjacent notches. Specifically, the optical carrier located at the midpoint of two notches ($\omega_0 = \omega_{0n}-0.5$ FSR) fails to obtain RF signal from the PD because of the symmetry of the MRR spectrum. In contrast, the optical carrier that moves toward one of the notches brings about the further separation of the center frequencies of the above-mentioned two sub-MPFs, which enlarges the passband bandwidth formed by their superposition. The RF response on the PD continues to exist until the optical carrier moves to the notch ($\omega_0 = \omega_{0n}$). Given the symmetry of the MRR spectrum, the variation of the MPF passband is symmetrical with that in the range of $\omega_{0n}-0.5$FSR to $\omega_{0n}$ when the frequency of the optical carrier lies in the $\omega_{0n}$ to $\omega_{0n}+0.5$FSR range.

Fig. 2(a) verifies the absence of RF response on MPF both at $\omega_e = 0$ and FSR. When the RF frequency $\omega_e = 0$ or FSR, the amplitude response and phase response of the MRR received by the carrier and the two bands are equal, which are $T(\omega_0) = T(\omega_0 \pm \omega_e)$ and $\Phi(\omega_0) = \Phi(\omega_0 \pm \omega_e)$. According to (4), the $i_{RF} \equiv 0$, which indicates that the frequency points $\omega_e = 0$ and

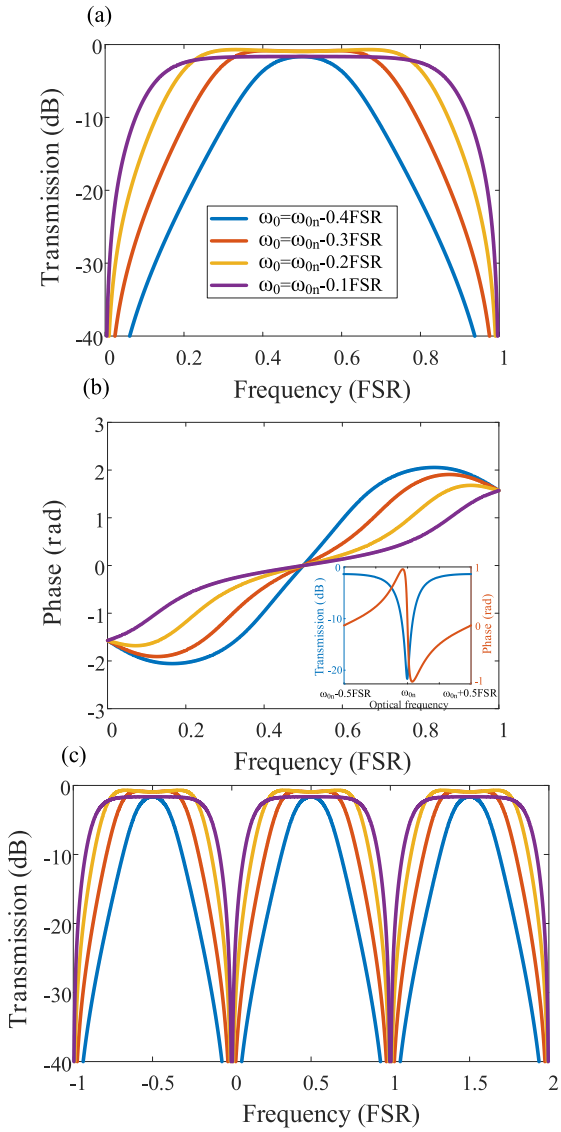


Fig. 2. Simulation results of RF response of MPF when the frequency offset of the optical carrier is different. The result of amplitude response (a) and phase response (b) Within an FSR range when $\alpha = 0.65$, t = 0.7. The result of amplitude response within 4 FSR range when $\alpha = 0.65$, t = 0.7(c). Inset: (b) The optical spectrum of MRR in an FSR range.

$\omega_e$ = FSR are within the stopband of the MPF. Such property results in a high out-of-band rejection ratio of the proposed MPF.

Owing to the periodic distribution of the MRR notches, the growth of the $\omega_e$ gives rise to the periodical presence of the passband in the frequency domain with a period of FSR. The center frequency of the Nth passband is (N-0.5)×FSR. Fig. 2(c) illustrates the simulation results. The analysis of each passband and stopband is the same as above.

## III. Experimental Results and Discussion

A proof-of-concept experiment is performed according to the setup in Fig. 1(a). A continuous-wave (CW) light from TLS (EXFO FLS-2800) is injected into the PM (ixblue MPZ-LN-40) with electro-optical bandwidth and insertion loss of 33 GHz and 2.5 dB, respectively. The optical carrier is first phase modulated

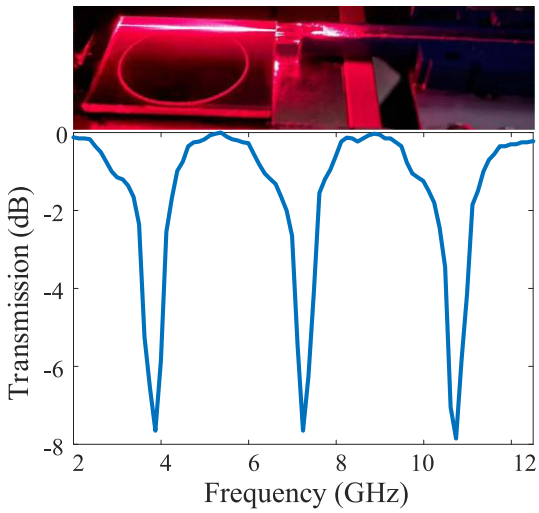


Fig. 3. The transmission spectrum of MRR.

by the RF signal from the VNA (Anritsu MS46322B) port 1 with an RF power of 5 dBm, and then is input into a $SiO_2$ MRR. After that, the optical carrier is beaten with two tailored sidebands on a high-speed PD (KG-PD-50G) with 3 dB bandwidth and responsibility of 50 GHz and 0.65 A/W. Finally, the photocurrent is sent to port 2 of the VNA and the transmission spectrum of the proposed MPF is obtained.

A strongly coupled MRR, which is essential for the proposed MPF as an optical filter, is designed and fabricated with a diameter 18 mm in order to complete the experiment. A core made of $GeO_2$+$SiO_2$ is embedded into the $SiO_2$ cladding. The refractive index of the cladding is 1.4442 at 1550 nm wavelength, and the relative refractive index difference between waveguide and cladding is 0.75%. In order to reduce the loss coupled with single-mode fiber and ensure the waveguide's sole support of single-mode transmission, both the width and height of the waveguide are designed to be 6 $\mu$m, which guarantees the insensitivity of waveguide to polarization. The insertion loss is about 4 dB. A 50:50 power division design is adopted in the coupling region, which means that a relatively large coupling coefficient k (about 0.7) is obtained due to the relation $t^2+k^2=1$ under ignoring coupling loss. The round-trip transmittance $\alpha$ can be written as [24]

$$\alpha \approx \left[1 - \frac{\pi \times \left(1+\sqrt{T_0}\right) \times \Delta f}{FSR \times L}\right]^{L/2} \tag{5}$$

where $T_0$ represents the fraction of transmitted optical power, and $\Delta f$ the 3 dB bandwidth of notches. The optical spectrum analyzer (OSA, Yokogawa AQ6317C) in the laboratory fails to characterize the accurate bandwidth of MRR owing to its maximal resolution bandwidth of 0.01 nm, so the transmission spectrum of the MRR is measured by tuning the wavelengths of laser in a step of 1pm and recording the optical power through optical power meter. The transmission spectrum and the photo of the coupling test with red light of MRR are shown in Fig. 3. The FSR, $T_{0,}$ and $\Delta f$ stand at 3.45 GHz, 0.18, and 0.65 GHz, respectively, thus $\alpha$ is estimated to be 0.65 and the Q

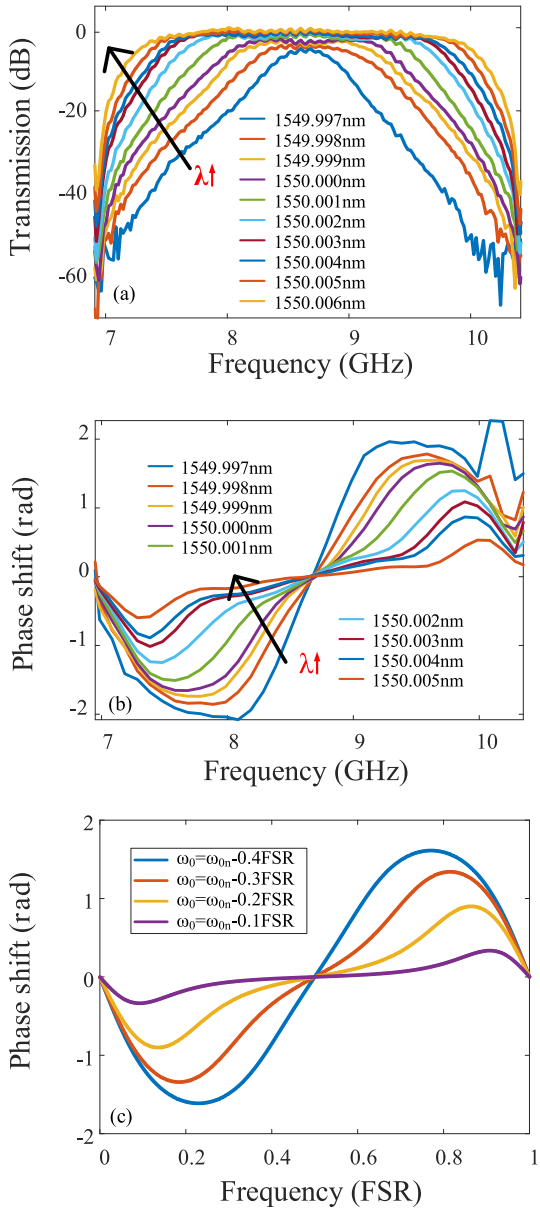


Fig. 4 The transmission spectrum of the MPF with different optical carrier wavelengths (a). The phase shift of MPF with different optical carrier wavelengths by experiment (b) or simulation (c).

factor(Q = $\lambda\Delta f$/c) is about 300000. The MRR is fabricated by plasma-enhanced chemical vapor deposition (PECVD).

To show the changing process of passband more clearly, Fig. 4(a) illustrates the normalized transmission spectrum of the proposed MPF for one passband. The wavelength of the optical carrier is tuned from 1549.997 nm to 1550.006 nm, with the minimum tuning step of 1 pm. When the wavelength of the optical carrier is set to 1549.997 nm, the optical carrier is closed to the center of two notches with a relatively narrow bandwidth of the MPF (0.73 GHz). The normalized amplitude of the MPF is $-5$ dB and the shape factor is 5.06 where the shape factor is the ratio of the 40 dB bandwidth to the 3 dB bandwidth. When the optical carrier further deviates from the center of two adjacent notches, the amplitude of the MPF gradually climbs and the

bandwidth increases in a step of around 0.25 GHz, resulting in a sharper transition band and the presence of flattop. When the wavelength of the optical carrier moves to 1550.006 nm, the optical carrier approaches one of the notches, and the bandwidth and normalized amplitude of the MPF mount to 2.73 GHz and 0 dB, respectively. The mechanism of PM-IM conversion is the main cause of monotonically increasing filter amplitude in tuning the wavelength. The shape factor is improved to 1.38. The experimental results share the simulation results in Fig. 2(a).

Given the effect of the linear phase response of VNA, a method for calibrating is required to establish reference planes for phase response measurement, which is usually realized with calibration kits. A simpler method is to take the MPF phase response at a certain optical carrier frequency as the reference plane and make a difference between the MPF phase response measured at other optical carrier frequencies and the reference plane to obtain the phase shift (the MPF phase response at 1550.006 nm serves as the reference plane), thus clarifying the changing trend of the MPF phase shift response with the optical carrier changes, as shown in Fig 4(b). According to the theory in the second part, the MPF phase response under the optical carrier frequency offset of −0.05 FSR is taken as the reference plane and the phase shift simulation results of the MPF under different carrier frequencies are obtained, as shown in Fig. 4(c). The experiment results support the simulation results.

Fig. 5 illustrates the multiband MPF electrical spectrum. The center frequency of the Nth passband records 3.45×(N-0.5) GHz, and the frequency of the Nth 0 response point is 3.45×(N-1) GHz. The movement of the optical carrier is followed by the synchronous change of the bandwidth of each passband, which supports the simulation results in Fig. 2(c). The experimental data and the fitting curve of each passband verify good consistency between passbands. The amplitude of the passband dips at high frequency due to the degradation of the S21 response of electrical and optoelectronic devices (including PM, PD, and cables) with growing frequency. This also means that the number of passbands can be reconfigured by utilizing the above-mentioned devices with appropriate working bandwidth. In addition, adding an optical filter to the link can also reconfigure. The stopband of the grating can filter out the repeated notches of MRR, as shown in points A and B in Fig. 1(b). Fig. 6 experimentally shows the normalized transmission spectrum of the MPF after adding a circulator and a grating with 3 dB bandwidth of 0.08 nm in the link where the inset shows the optical spectrum of the grating. The wavelength of laser is set at 1549.928 nm which is also the center wavelength of the grating. A single passband filter is achieved and the bandwidth is tuned by changing the temperature of MRR. The experimental results confirm the reconfigurability of the multiband MPF. However, limited by the fabrication deviation, the out-of-band rejection ratio (<25 dB at 0.25 nm away from the center wavelength) and roll-off of the grating does not perform as expected, which means that the excess passbands cannot be deeply suppressed. Besides, the spectral asymmetry of grating introduces interference for phase-modulated signal so the out-of-band frequency response of MPF is improved. The two mentioned factors degrade the out-of-band ratio of MPF.

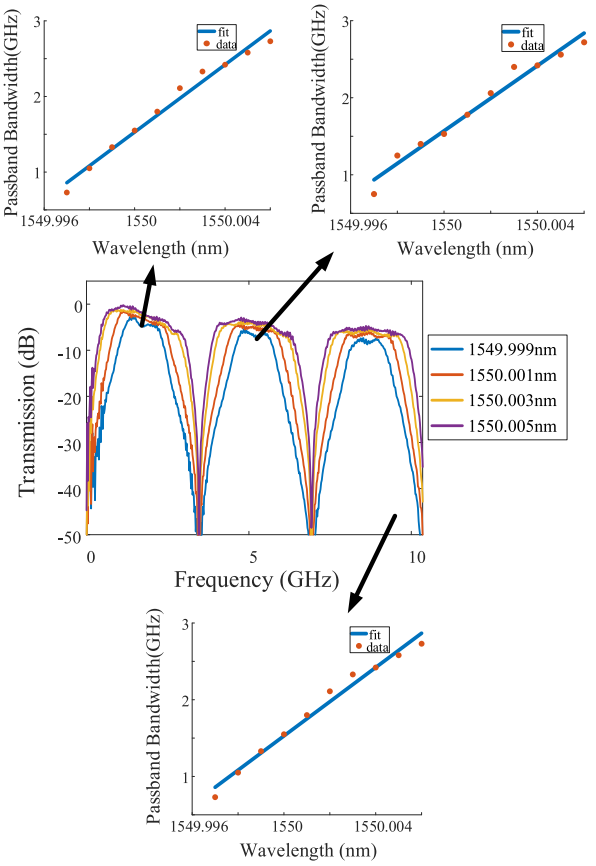


Fig. 5. Experimental result of multiband MPF transmission spectrum.

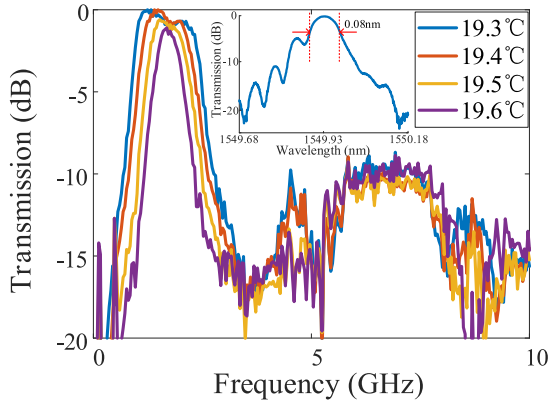


Fig. 6. Realization of single-band MPF by adding optical filter with narrow bandwidth in the link. Inset: The optical spectrum of the grating.

Moreover, the center frequency of each passband of the multiband MPF only determined by the FSR of MRR, so it is not susceptible to the external interference, which makes it suitable for multi-frequency scenarios with fixed operating frequencies.

## IV. Conclusion

In conclusion, a photonic-based bandwidth tunable multiband filter is proposed and experimentally demonstrated. Theoretical analysis has been carried out to describes the implementation of a strongly coupled MRR, acting as an optical spectrum tailored

to achieve multiband MPF by PM-IM conversion. The optical carrier and its two adjacent notches form a bandpass filter superimposed by two sub-MPFs, where the center frequency is 0.5 FSR and zero frequency response at DC and FSR. The relative position of the optical carrier and the two notches can be adjusted to change the overlapping frequency response of the two sub-MPFs, thus converting the bandwidth. Owing to the periodicity of the MRR transmission spectrum, multiple passbands arranged on the spectrum with FSR as the period are combined into a multiband MPF. The experiment performed a bandwidth reconfigurability of 0.73–2.73 GHz, and the shape factor was improved from 5.06 to 1.38. The number of passbands can be reconfigured by an optical filter. The proposed multiband MPF has the advantages of simple structure, high reliability, and integrability, which makes it have a broad application prospect in wireless communication and signal processing.

## REFERENCES


[1] R. Cavallari, F. Martelli, R. Rosini, C. Buratti, and R. Verdone, "A survey on wireless body area networks: Technologies and design challenges," *IEEE Commun. Surv. Tuts.*, vol. 16, no. 3, pp. 1635–1657, Jul.–Sep. 2014, doi: 10.1109/surv.2014.012214.00007.

[2] M. Brandolini, P. Rossi, D. Manstretta, and F. Svelto, "Toward multistandard mobile terminals-fully integrated receivers requirements and architectures," *IEEE Trans. Microw. Theory Techn.*, vol. 53, no. 3, pp. 1026–1038, Mar. 2005, doi: 10.1109/tmtt.2005.843505.

[3] S.-Z. Chen and S.-L. Kang, "A tutorial on 5G and the progress in China," *Front. Inf. Technol. Electron. Eng.*, vol. 19, no. 3, pp. 309–321, 2018, doi: 10.1631/fitee.1800070.

[4] S. Holme, "Multiple passband filters for satellite applications," in *Proc. 20th AIAA Int. Commun. Satell. Syst. Conf. Exhib.*, 2002, Art. no. 1993.

[5] A. Othman, R. Barrak, and M. Mabrouk, "A multiband filter for multistandards wireless communications receivers," *Radioengineering*, vol. 27, no. 1, pp. 193–199, Apr. 2018, doi: 10.13164/re.2018.0193.

[6] S. F. R. Chang et al., "A dual-band RF transceiver for multistandard WLAN applications," *IEEE Trans. Microw. Theory Techn.*, vol. 53, no. 3, pp. 1048–1055, Mar. 2005, doi: 10.1109/tmtt.2005.843509.

[7] M. A. Abdalla, A. M. Ahmed, and A. M. M. Allam, "A multiband filter for wireless and RFID applications," in *Proc. Int. Conf. Eng. Technol.*, German Univ. Cairo, Cairo, Egypt, 2014, pp. 1–4.

[8] A. G. Dempster, "Use of comb filters in GPS L1 receivers," *GPS Solutions*, vol. 12, no. 3, pp. 179–185, 2007, doi: 10.1007/s10291-007-0079-3.

[9] M. P. Fok, J. Ge, Q. Liu, E.-H. Lee, and S. He, "Dynamic and multiband RF spectral processing," *Proc. SPIE*, vol. 10922, pp. 105–113, 2019.

[10] L. Liu, X. Jin, T. Ning, L. R. Chen, and J. Capmany, "Dual-frequency optoelectronic oscillator incorporating a single cavity and multiband microwave photonic filter," *Opt. Exp.*, vol. 29, no. 9, pp. 14006–14015, Apr. 2021, doi: 10.1364/OE.423148.

[11] S.-C. Pei, Y.-D. Huang, S.-H. Lin, and J.-J. Shyu, "Design of variable comb filter using FIR variable fractional delay element," *Signal Process.*, vol. 92, no. 10, pp. 2409–2421, 2012, doi: 10.1016/j.sigpro.2012.03.001.

[12] J. Mora, L. R. Chen, and J. Capmany, "Single-bandpass microwave photonic filter with tuning and reconfiguration capabilities," *J. Lightw. Technol.*, vol. 26, no. 15, pp. 2663–2670, Aug. 2008, doi: 10.1109/jlt.2008.927596.

[13] B. Vidal, M. A. Piqueras, and J. Martí, "Tunable and reconfigurable photonic microwave filter based on stimulated Brillouin scattering," *Opt. Lett.*, vol. 32, no. 1, pp. 23–25, 2007.

[14] L. Xu et al., "Silicon-on-insulator-based microwave photonic filter with widely adjustable bandwidth," *Photon. Res.*, vol. 7, no. 2, pp. 110–115, 2019, doi: 10.1364/prj.7.000110.

[15] M. Fok and J. Ge, "Tunable multiband microwave photonic filters," *Photonics*, vol. 4, no. 4, pp. 45–64, 2017, doi: 10.3390/photonics4040045.

[16] L. A. González-Mondragón, L. J. Quintero-Rodríguez, A. García-Juárez, A. Vera-Marquina, and I. E. Zaldívar-Huerta, "Multiple passband microwave photonic filter with adjustable bandwidth," *Opt. Laser Technol.*, vol. 126, pp. 106133–106140, 2020, doi: 10.1016/j.optlastec.2020.106133.

[17] L. Liu, X. Jin, T. Ning, L. R. Chen, and J. Capmany, "Optical spectral slicing based reconfigurable and tunable microwave photonic filter," *J. Lightw. Technol.*, vol. 38, no. 19, pp. 5492–5499, Oct. 2020, doi: 10.1109/jlt.2020.3009616.

[18] W. Bogaerts et al., "Silicon microring resonators," *Laser Photon. Rev.*, vol. 6, no. 1, pp. 47–73, 2012, doi: 10.1002/lpor.201100017.

[19] Z.-C. Guo, G. Zhang, Y.-P. Lyu, and L. Zhu, "Multiband waveguide filters with compact size and large frequency ratio," *IEEE Trans. Plasma Sci.*, vol. 50, no. 3, pp. 761–766, Mar. 2022, doi: 10.1109/tps.2021.3133295.

[20] R. Gomez-Garcia, R. Loeches-Sanchez, D. Psychogiou, and D. Peroulis, "Multi-stub-loaded differential-mode planar multiband bandpass filters," *IEEE Trans. Circuits Syst. II: Exp. Briefs*, vol. 65, no. 3, pp. 271–275, Mar. 2018, doi: 10.1109/tcsii.2017.2688336.

[21] E. Musonda, R. A. Paradkar, I. C. Hunter, and R. Parry, "Synthesis of multiband filters by linear optimization," *IEEE Trans. Microw. Theory Techn.*, vol. 67, no. 12, pp. 4764–4772, Dec. 2019, doi: 10.1109/tmtt.2019.2945755.

[22] Y. Chen and Q. Qiu, "A novel microring resonator based on multi-Mach–Zehnder interferometers," *Opt. Commun.*, vol. 483, pp. 126643–126649, 2021, doi: 10.1016/j.optcom.2020.126643.

[23] W. R. McKinnon et al., "Extracting coupling and loss coefficients from a ring resonator," *Opt. Exp.*, vol. 17, no. 21, pp. 18971–18982, 2009.

[24] L.-W. Luo, G. S. Wiederhecker, J. Cardenas, C. Poitras, and M. Lipson, "High quality factor etchless silicon photonic ring resonators," *Opt. Exp.*, vol. 19, no. 7, pp. 6284–6289, 2011, doi: 10.1109/PGC.2010.5706128.